The influence of Fe and Mn content and cooling rate on the microstructure and mechanical properties of A380-die casting alloys

S. Seifeddine, I. L. Svensson
Jönköping University, School of Engineering Component Technology - Jönköping - Sweden

ABSTRACT

In the present investigation, the microstructure and tensile properties of aluminium die-cast alloys, based on A380, are studied in details as a function of the iron and manganese content and solidification rate. One set of experiments was designed to examine the "solely" effect of Fe content, which varied from 0.1 up to 1.6 wt % and another set with manganese additions, Mn:Fe ~ 1:2. Three solidification rates corresponding to ~ 10, 25 and 60 μm in secondary dendrite arm spacing, SDAS, respectively were employed by using the unique gradient solidification technique. Microstructure analysis reveals that at relatively high cooling rates and iron levels, the iron-rich precipitates are suppressed to some extent and the strength is maintained at high levels, but the ductility is gradually decreased. The amount of iron-rich intermetallics does not appear to influence the size and area fraction of porosity and consequently the result suggests that tensile properties have not been adversely affected by porosity level. These results offer additional insight into commonly discussed microstructure features and their role in the determination of the quality and soundness of Al-Si cast alloys.

RIASSUNTO

Nel presente lavoro vengono studiate in dettaglio la microstruttura e le proprietà tensili di una lega di alluminio per pressocolata della famiglia A380, in funzione del contenuto di Ferro e Manganese e della velocità di solidificazione. Il primo gruppo di esperimenti è stato rivolto unicamente a valutare l'effetto del contenuto di Fe, variabile dallo 0,1 al 1,6% in peso, mentre il secondo considera l'aggiunta di Mn nel rapporto Mn:Fe ~ 1:2. Sono state utilizzati tre livelli di velocità di raffreddamento, corrispondenti indicativamente a valori di 10, 25 e 60 μm della spaziatura dendritica secondaria, SDAS, utilizzando una tecnica di solidificazione a gradiente. L'analisi microstrutturale rileva che in presenza di elevati gradienti di raffreddamento ed alti livelli di Fe, i precipitati di fasi ricche in Fe vengono parzialmente eliminati e la resistenza del materiale si mantiene su livelli elevati, ma si riduce progressivamente la duttilità. La quantità di intermetallici ricchi in Fe non sembra influenzare la dimensione e la porosità percentuale e, di conseguenza, il risultato suggerisce che le proprietà tensili non sono state influenzate negativamente dal livello di porosità. Questi risultati offrono una possibile nuova chiave di lettura delle caratteristiche microstrutturali comunemente considerate e della loro influenza sulla qualità e sulla sanità metallurgica di getti realizzati con leghe Al-Si.

KEYWORDS

Al-Si based alloys; secondary dendrite arm spacing, iron-rich intermetallics; mechanical properties; defect formations.

INTRODUCTION

In commercial aluminium production, Fe and other impurities are unavoidable, especially when dealing with recycled materials. Iron is recognized as the most detrimental impurity due to the formation of brittle intermetallics called iron-rich platelets recognized as the β-Al_5FeSi needles. The sharp tips of these needles are acting as stress raisers which are progressively decreasing the ductility and ultimate tensile strength. Considerable studies have been reported regarding the formation of Fe-bearing phases in relation to the iron content and cooling rate [1-14]. Concerning the effect of iron content on the formation of Fe-bearing compounds, many researches have reported that at 0.05%<Fe<0.7% a small needle-like phase is believed to form after the eutectic Si, along with Si, in a ternary eutectic reaction. At these levels of iron, the tensile strength did not seem to be remarkably influenced except the elongation that suffered an essential reduction [13]. At Fe> 0.7 % most of Al_5FeSi -needles seems to be precipitated prior to the eutectic Si [7, 8, 12]. Lu et al. [7] concluded that higher iron levels not only did enhance the total amount of Al_5FeSi -needles but also shifts to precipitation sequences of this phase to higher temperature resulting in extremely coarse needles. Even if the iron level is quite low, enough iron segregates during solidification to cause the β-Al_5FeSi -needles to form. At high cooling rates, as in the case of high pressure die casting, the occurrence of primary Al_5FeSi -needles is shifted towards higher iron levels, Fe>1%. Varying the iron content from 1 up to 1.8 %,

[14], successively resulted in a serious reduction of the tensile strength and also the elongation.

In order to enhance the overall properties such as tensile, fatigue and corrosion properties, the morphology of the iron-rich β-Al_5FeSi-needle is required to be altered to a more compact, less harmful intermetallic compounds such as the α-$Al_{15}(Fe,Mn)_3Si_2$ having a Chinese script morphology. Shabestari et al. [15, 16] has reported that alloying with 0.9% Mn, resulted in apparent fragmentation of the β- Al_5FeSi -needles. At higher Mn levels the plate-like morphology of the β-Al_5FeSi -needles was replaced by $Al_{15}(Fe,Mn)_3Si_2$-dendrites in the form of plate, polyhedral or star-like shapes. In the absence of Mn, the increase in cooling rate and decrease in iron content results in size and volume fraction reduction of Al_5FeSi -needles and a finer dispersion of these particles is appeared [3, 4, 6]. Besides their detrimental influence on the mechanical properties, the precipitation of binary β-phases is proposed to block the feeding channels of the interdendritic network earlier. Several researchers have investigated the impact of iron on the porosity formation in Al-Si cast alloys [7, 11, 12, 17-26]. According to Lu et al. [7], at low iron contents (Fe<0.3%) sponge-like pores have been detected in the centre of the casting which is suggested to be formed due to the presence of ternary β platelets. At iron levels 0.3% up to 0.7% the level of porosity is still as for the levels mentioned earlier but distributed across a wider area. Other related research demonstrate that an increase in porosity are detected at intermediate iron contents (Fe>0.4%). Furthermore, it is suggested that at higher iron contents (Fe>0.7%), the β platelets have been observed to participate in the nucleation of eutectic silicon [12, 18, 19, 27], therefore leading to a rapid deterioration of the interdendritic permeability resulting in shrinkage cavities, which is in disagreement of what Lu and Dahle [7] have reported. A number of aspects mentioned above, require further investigation and the present research attempts to investigate the influence of varying the cooling rate, Fe and Mn concentration on the microstructure (intermetallic compounds and porosity) and mechanical properties of an Al-9%Si-3%Cu alloy produced by gradient solidification technology. This study differs from previous research in a number of respects: specimens of different microstructure coarsenesses are directionally solidified, with a homogeneous and well-fed microstructure throughout the entire sample accompanied with low levels of casting defects such as oxide films, shrinkage porosity etc; thereby revealing the inherent potential of the examined alloys.

EXPERIMENTAL

MELT PREPARATION AND PROCESSING TECHNIQUES

The chemical composition of the alloys prepared for the current study is shown in table 1. The alloys were produced by adding Si, Cu, Fe, Mn and Sr to the aluminium melt. When it comes to Fe and Mn, they were added in powder form with a purity of 75% respectively; the remaining 25% is flux media. The resistance furnace was set to 750°C and the alloying elements were preheated to 200°C.

In order to simulate various casting processes, a gradient solidification furnace was used. The furnace works by holding a metal specimen in a heated environment until it is fully melted, protected from oxidation by the use of an argon gas shield. The temperature was set to 710°C and the samples were left at that temperature for 20 minutes. The furnace is raised at a prescribed speed while the metal sample stays in a stationary position. At the base of the rising heating chamber there are jets of water which cool the metal specimen as it passes by. By changing the speed of the heating element, different microstructures can be obtained, but in this study three solidification rates are regarded which correspond to ~10, 25 and 60 μm SDAS respectively.

Table 1. Actual composition of the alloys that have been used in this investigation.

		Main elements (%)				
	Alloy	Si	Cu	Fe	Mn	Fe/Mn
Set I	1	9.9	2.8	0.15	0.00	
	2	9.5	3.0	0.29	0.00	
	3	9.6	2.9	0.48	0.00	
	4	8.5	3.0	0.85	0.00	
	5	10.3	2.9	0.99	0.00	
	6	9.4	2.7	1.30	0.00	
	7	9.3	2.6	1.60	0.00	
Set II	8	9.6	2.8	0.35	0.15	2.3
	9	9.3	2.7	0.79	0.34	2.3
	10	9.8	3.2	1.10	0.50	2.2
	11	9.2	3.0	1.59	0.79	2.0

TENSILE TESTING AND SAMPLE PREPARATION FOR THE MICROSCOPIC INVESTIGATION

From the gradient solidification furnace, the samples had to be machined to the proper profile for tensile testing. A CNC-lathe was employed for accurate and repeatable contours to each of the samples, see figure 1. The tensile tests were conducted one week after the specimens were produced by using a tensile test device called Lloyd EZ50.

Tension was accomplished by increasing tension load until it resulted in specimen fracture; the strain rate was 0.5 mm/minute. Strain was measured using an axial extensometer with a gage length of 25 mm. Macro Vickers hardness

measurements have also been carried out on the tensile tested samples. An average over five readings is taken to assess each hardness value presented for each specimen and condition. To quantify microstructural features, SEM, EDS and optical microscopy with image processing software were used. If nothing else stated, all microstructural phases presented are identified by their colour and morphology. The average length of SDAS taken over 20-30 readings in each case, the average maximum length of the Fe-rich intermetallics covering the entire sample surface including the longest 20-30 needles, and the average maximum length and percentage area fraction of porosity were examined.

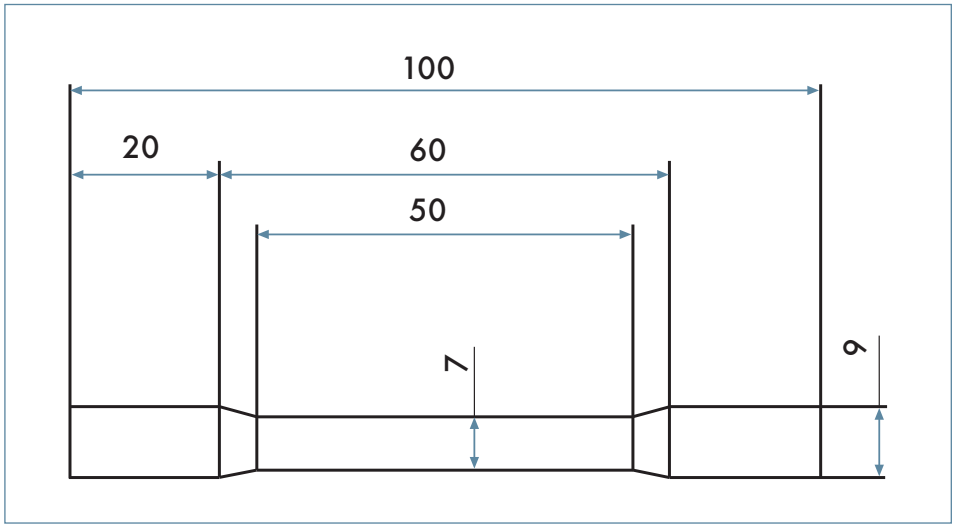

Fig. 1: A schematic illustration of the tensile test specimen [mm].

RESULT AND DISCUSSION

MICROSTRUCTURE ANALYSIS

As shown in figure 2 a-c, d-f and g-i, three different microstructures have been achieved. The microstructure coarsenesses have been measured as the distance between the secondary dendrite arm spacings, SDAS, which is a function of the cooling rate, but often preferred to the solidification time as an indicator of the solidification conditions in the castings [28]. As clearly demonstrated, the smaller the SDAS the finer and more homogenous is the microstructure and vice versa. It can be noted that the Al-Si eutectic for the samples with longer SDAS is more of a flake like morphology and not as fibrous as in the case of the samples produced at higher cooling rates even though they are all modified by Sr.

Generally, it seems that at high cooling rates and iron levels up to 0.8%, the precipitates of iron-rich needles with stoichiometry Al_5FeSi, is few and evenly distributed, see the optical micrographs in figure 2 a-i where the microstructure of three different levels of iron and cooling rates are presented. As the cooling rate is reduced larger precipitates are formed and distributed randomly. The volume fraction, length and width of theses precipitates are likely to be escalated as the SDAS as well as the iron content are increased.

As depicted from figure 2 f and i, the iron-rich needles are formed as coarse and large platelets and rods. According to Lu et al. [7], at iron levels above 1%, the iron needles precipitate as primary and result in extremely large structures independent of the cooling rate. At lower iron levels <0.8%, the iron needles precipitate at lower temperatures along with development of Si-eutectic as a ternary reaction after the Al-Si eutectic has been formed. As an outcome, the needles, or as they also might be denoted as β-phase, tend to become short and fine and are usually distributed in the eutectic regions, but might also crystallizes along the interdendritic arms.

Shabestari [16] also reported that these needles tend to be very hard and brittle and have relatively low bond strength to the matrix: iron correctors are usually used in order to convert their morphology and crystal structure. As a neutralizer, Manganese is often added to reduce the embrittlement and to alter the shape from

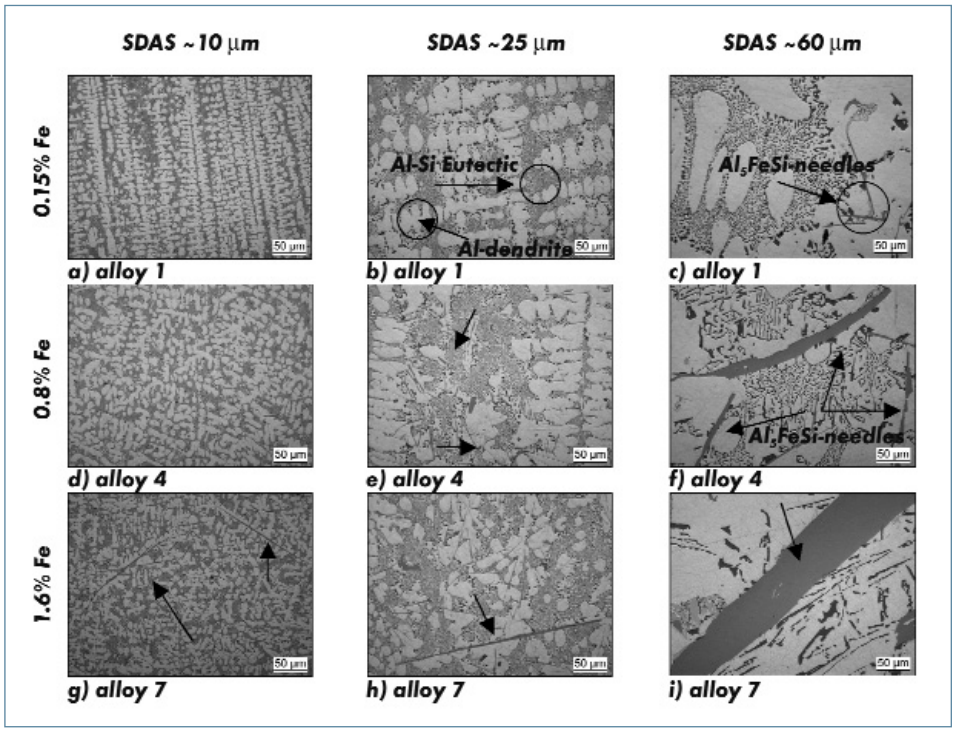

Fig. 2: Microstructures illustrating the effect of the cooling rate and iron concentrations in Al-Si alloys.

sharp needles to a more compact type, which is more or less equiaxed and tending to form as dendrites with a Chinese script like morphology, α-phase, with a stoichiometry that corresponds to $Al_{15}(Fe,Mn)_3Si_2$.

In order to control and understand the morphology of iron compounds that precipitate during the solidification, Mn has been added and the Mn:Fe ratio was maintained at 1:2 [4]. There is still disagreement in literature whether Mn totally modify or nullify the iron-rich needles or not, [4, 15-16] and according to the present investigation, see figure 3 a-f, the iron-rich needles Al_5FeSi are always present and coexisting with α-phase $Al_{15}(Fe,Mn)_3Si_2$ as long as iron and manganese are present.

The morphology of the α-phase is seen to alter from Chinese-script type to a more coexisting star-like and polyhedral type as the iron level is increased as seen in figure 3 f. As the level of iron and/or manganese is increased, volume fraction, coarser and more complex intermetallics are likely to develop and the size of each of them seem to be a function of the cooling rate and of the Fe and Mn level in the melt; as they might precipitate as post dendritic and/or as pre- or post-eutectic [29].

The results of the average length of the iron-rich needles are listed in table 2 and related to the level of iron in the alloys, SDAS and to the level of "neutralizer" Mn. Due to the shape of Chinese script α-phase, the area of the compact iron-rich region has been measured instead of the length.

As indicated from table 2, the length of the needles is remarkably increased as the iron and solidification time in terms of SDAS is increased. Despite of maintaining the ratio Mn:Fe ~1:2, the size and volume fraction of the α-phase Chinese scripts is increased as a function of the cooling rate and Fe and Mn additions. At relatively high cooling rates, SDAS ~7-10 μm, no Chinese script morphologies were detected until the level of iron exceeded 1%; instead some small polyhedral particles has been observed, few in numbers and finely distributed. Generally, it seems that when adding Mn, the alloys display shorter iron-rich needles which might be due to less amount of iron available in the melt, since the formation of Chinese script and other intermetallics are promoted as well. As an outcome, a strong relationship appears to exist between the

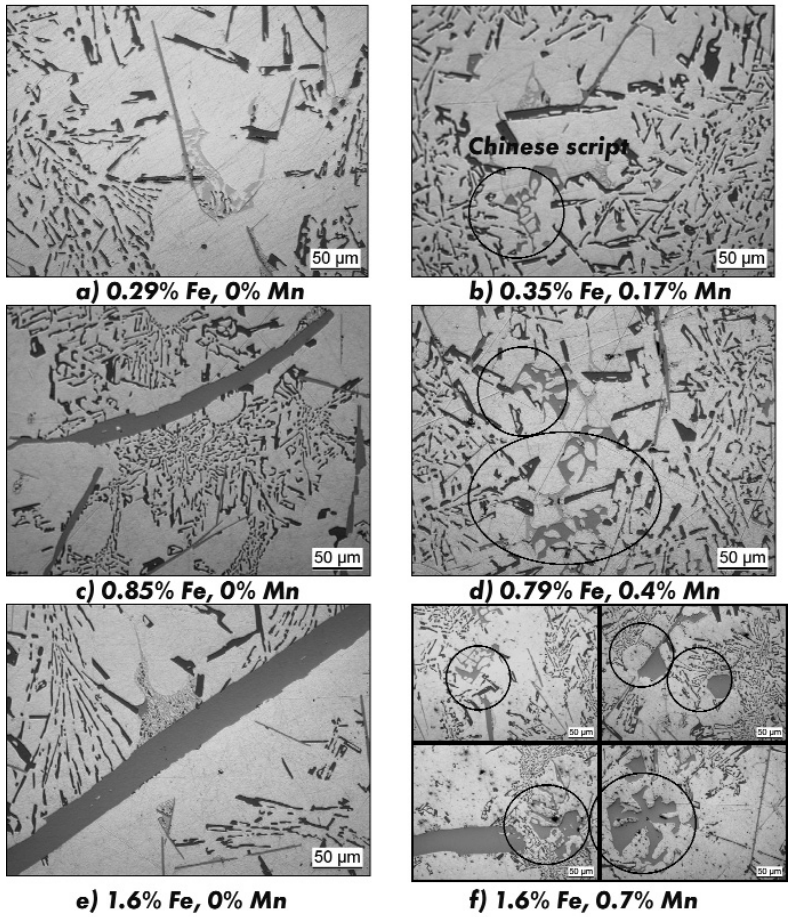

Fig. 3: Microstructures of Fe and Fe/Mn containing Al-Si alloys with SDAS of ~60μm.

Table 2. Demonstration of the progressive increase and coarsening in length and area of the iron compounds in relation to the solidification rate expressed in term of SDAS.

		Maximum Al5FeSi-needle length (μm)			Maximum Al15(Fe,Mn)3Si2-Chinese script area (_m2)		
Fe conc. w(%)	Mn conc. w(%)	SDAS: 7-10 μm	SDAS: 20-25 μm	SDAS: 50-60 μm	SDAS: 7-10 μm	SDAS: 20-25 μm	SDAS: 50-60 μm
0.29		4	80	295			
0.85		73	210	669			
1.30		120	296	1370			
1.60		388	584	3366			
0.35	0.15	5	45	268		129	1209
0.79	0.34	72	100	378		157	2852
1.10	0.50	77	287	317		2741	46559
1.59	0.79	279	548	1221	640	1985	13359

SDAS and the average length and area of the iron-rich compounds, see table 2.

Energy dispersive spectrometry analysis (EDS), of the β-phase, and the α-phase from samples taken from alloys 4 and 11, clearly confirm that some Mn is found in the iron-rich needles when Mn is present in the melt. It seems that during the precipitation of the β-phase, which seems to be very hard to control no matter if Mn is present or not in the melt,

Mn is tied up and participated in the formation of these needles; reducing the total amount of Mn available for converting β-phase into a α-phase. The chemical composition of the precipitates seem to differ slightly from what reported in literature [9, 16, 30- 31].

Remark, at higher Fe and Mn levels, sludge formation might be taking place due to an improper melt handling process and high levels of Fe, Mn and Cr exceeding the recommended sludge factor. Calculation of the sludge factor is discussed in details elsewhere [3, 15]. Some trace elements of Cr might be present in small concentrations and, perhaps, instead of converting the iron-rich needles into a more compact morphology, the Fe, Mn and Cr might have precipitated as sludge, which should absolutely be avoided since its presence might be deleterious to the overall properties.

Regarding the relation between the iron level and nucleation and formation of porosity, several researchers have devoted a lot of research in understanding the relationship and the role of iron Al-Si cast alloys [7, 11-12, 17-26]. Iron facilitates the formation of porosity which seems to be associated with the formation and occurrence of iron intermetallics. The iron intermetallics are expected to cause severe feeding difficulties during solidification. The morphology of the β-phase blocks the interdendritic flow channels, why it is proposed that higher iron contents in the alloy is associated with higher levels of porosity. Similar observations have been detected, see figure 4a, but concerned only alloys with iron levels >1% and longer solidification times, which mainly seem to be related to the primary precipitation of iron-rich β-phase that tends to grow and coarsen; being as flakes leading to this kind of micro porosity. Since the microstructure of these specimen are well fed, less frequent is this kind of phenomena since the orientation and growth of these needles are randomly directed.

In the present study, it has been observed that the cooling rate, SDAS, seems to govern the length as well as the percentage area fraction of porosity. Generally, it appears that a reduction in SDAS results in smaller average pore size and a reduced area fraction of porosity and vice versa, see table 3. Worth to indicate is that the melt hydrogen content has not been

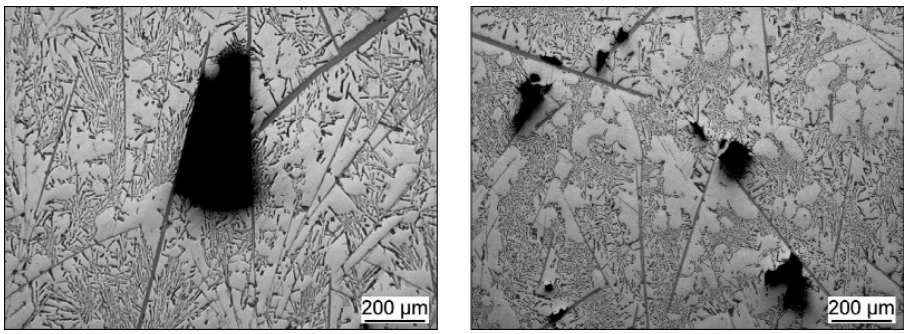

Fig. 4: Optical micrographs illustrating the porosity formation adjacent to the β-phase in alloy 6 with 1.3%Fe and SDAS ~60µm: a) β-phases blocking the interdendritic flow and b) possible pore nucleation on the β-phase.

measured and assumed in this case to be constant for all the alloys since they have been produced under similar conditions. It is obvious that as the solidification time is low, less time will therefore be available for the diffusion of the hydrogen into the interdendritic regions which results in small sizes of pores.

A theory, that involves the harmfulness of the oxide films, suggests that when an oxide particle is approached by the solidification front, the particle experiences the hydrogen-rich environment produced by the rejection of gas from the advancing solid. Furthermore, the access of gas by diffusion into the air pocket in the gap of the oxide particles, the pore will starts to form and grow. As the freezing rate is slow and the particle is poorly wetted by the melt, time will therefore be available for more hydrogen to diffuse resulting in pore expansion and growth, [33-34]. But comparing the porosity formation, the samples with SDAS ~ 20-25 µm are associated with largest percentage area fraction of porosity which might be due to the arrestment of premature pores as they become entrapped by the advancing solidification front.

In the case of the larger SDAS ~60 µm, it is therefore reasonable to assume that due the slow cooling conditions many air pockets formed within the liquid, or due to interaction with oxide particles, has been driven in front of the solidified front without being engulfed and in that case not been detected in the gradient solidified specimens due to the solidification mode. Another reason might be the longer time available for the hydrogen to diffuse and move in front of solid-liquid interface out of the sample into the surrounding environment.

Studies made by Dinnis et al [17] indicates that the addition of Mn play an important role

Table 3. The maximum pore length and percentage area fraction of porosity for the alloys studied.

	Maximum pore length (µm)			Pore area fraction (%)		
Fe conc. w(%)	SDAS: 7-10 µm	SDAS: 20-25 µm	SDAS: 50-60 µm	SDAS: 7-10 µm	SDAS: 20-25 µm	SDAS: 50-60 µm
0.15	105	380	727	0.52	2.22	1.60
0.29	97	364	300	0.32	2.27	0.76
0.48	89	368	249	0.25	3.24	0.67
0.85	150	239	279	1.21	3.37	0.56
0.99	128	300	474	0.92	2.43	1.59
1.30	98	191	252	0.65	3.51	1.77
1.60	122	175	315	0.61	3.39	1.51

in reducing the amount of porosity in alloys with supercritical iron contents (Fe>1%). At higher amount of Fe>1% with no addition of Mn, the concentration of Fe in the liquid is sufficiently high due to the low solubility of iron in aluminium, the nucleation of β platelets occurs before the Al-Si eutectic reaction leading to coarser and larger iron intermetallics. The addition of small amount of Mn in relation to iron (Mn: Fe=1:6) seems to not influence the degree of porosity. At high Mn:Fe ratio (Mn:Fe = 1:2) the more compact α-phase forms early in the solidification process and a large amount of iron is therefore consumed, reducing the iron content of the residual liquid and preventing the nucleation of β platelets prior to the Al-Si eutectic leading to a reduction in porosity. The shape of these Chinese scripts facilitates the filling up of the metal in between the branches of these particles instead of the blocking mechanism induced by the needles.

Other related research demonstrate that an increase in porosity are detected at intermediate iron contents and that the β-phase participates in the nucleation of eutectic silicon [12, 18-19, 32], therefore leading to a rapid deterioration of the interdendritic permeability. Literature [11, 20-23] showed that an increase in iron content results in the precipitation of the β platelets with their branched morphology that promote an inability of the liquid metal to feed into the spaces between these branches leading to shrinkage cavities. It has also been suggested that the β- Al_5FeSi -needles are very active sites for pore nucleation, see figure 4b, and that addition of Mn, which inhibits the formation of these needles, also neutralizers the pore nucleation [22]. In the present investigation, the addition of Mn appears to influence neither the pore size nor the area fraction, since Mn seems not to suppress the formation of β-phase.

MECHANICAL PROPERTIES

The mechanical properties obtained from samples produced by the gradient solidification technique with three different microstructures and a wide variation of iron concentrations are presented in figure 5 a-f. As declared from figure 5a, the elongation to fracture seems to suffer a loss mostly by an increased iron level, independently of the cooling conditions. The fracture profile of smallest SDAS is of more intergranular character and the material is ductile, while for higher SDAS >50 μm the fracture surface seems to be more transgranular. The low ductility obtained with small SDAS is preferentially ascribed to larger volume fraction of iron-rich compounds that form as the iron level is increased. These particles are generally brittle why they tend to crack relatively early in the deformation process and consequently lowering the ductility. The reduction in elongation to fracture for the material with larger SDAS might be devoted to the larger Si particles with flake like morphology and, of course, to the large iron-rich needles or platelets. In most of all ductile materials that are subjected to monotonic loading, the progression of damage is devoted to the nucleation and growth of cracks. The release of stresses that is carried by the second phase particles such as the Si and intermetallic compounds, at a macroscopic level when cracking occurs affects the overall load bearing capacity of the material and governs the work hardening behaviour. There exists a relationship between damage and work hardening since the flow stress increase in the matrix leads to a higher level of load transfer to the second phase increasing the rate of damage development. This relationship between concurrent work hardening and damage development during deformation complicates often the analysis of these materials. Worth to bear in mind is that the damage events change the local stress distribution in the microstructure and the level of internal stresses by relieving stresses in the particles, due to tensile loading, might be reduced. On the other hand, the defect introduced by the damage, depending on its shape, may lead to higher local stress concentrations [35-36]. Exhibiting a size of several millimetres, these needles appear to participate in the damage events and play a critical role in the crack initiation and propagating processes, acting as easy crack paths, linking the particle fractures together and leading to an uncontrolled fracture of the material. The refining effect as a result of the higher cooling rate enabled the material to withstand higher deformation rates, why these materials exhibited higher ductility values.

The increase of the iron to levels >0,6% exerted an appreciable impact on the ultimate tensile strength, and the iron compounds are likely to act as reinforcing particles, see figure 5b. At higher iron levels, the length and volume fraction of iron compounds converted the trend and a negative relationship is clearly indicated. Otherwise, the yield strength, strength coefficient, see equation 1 (where σ is the true flow stress, *K* is the alloy's strength coefficient, ε is the true plastic strain and *n* the strain hardening exponent), and the macro Vicker´s hardness all are beneficially affected by the increase of Fe and cooling rates, figure 5c, d and f respectively.

$$\sigma = K\varepsilon'' \qquad (1)$$

Surprisingly, the strain hardening exponent, n, being as an indicator of the material ability to deform plastically, exhibited a positive influence as the iron level and its brittle compounds are increased in the material, figure 5e.

Porosity is often blamed for being very harmful and adversely impairing the mechanical properties and that poses a risk of occurrence of a premature failure, especially for parts with thin sections. Several authors have commented on the impact of porosity on the static tensile properties and there still exist a lot of disagreements whether the length of the pore, the area fraction or the volume fraction of porosity deleteriously influence the overall properties of Al-Si alloys [37-42]. As observed from the measurements that have been carried out in this investigation, porosity doesn't govern any of the presented mechanical properties. The reason might be that the iron-rich compounds exert a larger role on the fracture behavior and governs the fracture process, before any actual role of the porosity takes place. As shown in figure 6 a-c and d-f, the brittle Fe-rich needles appear to fracture as the stress is imposed. Even if it is reasonable to assume that the region of pores will yield first, affecting the yield strength, due to the reduced load bearing area concentrating the strain near the voids no fracture is occurred around the pore region. Parallel to the loading axis, the iron-rich β-platelets seem to fail at low applied strain during tensile loading, but due to the orientation of the cracks some

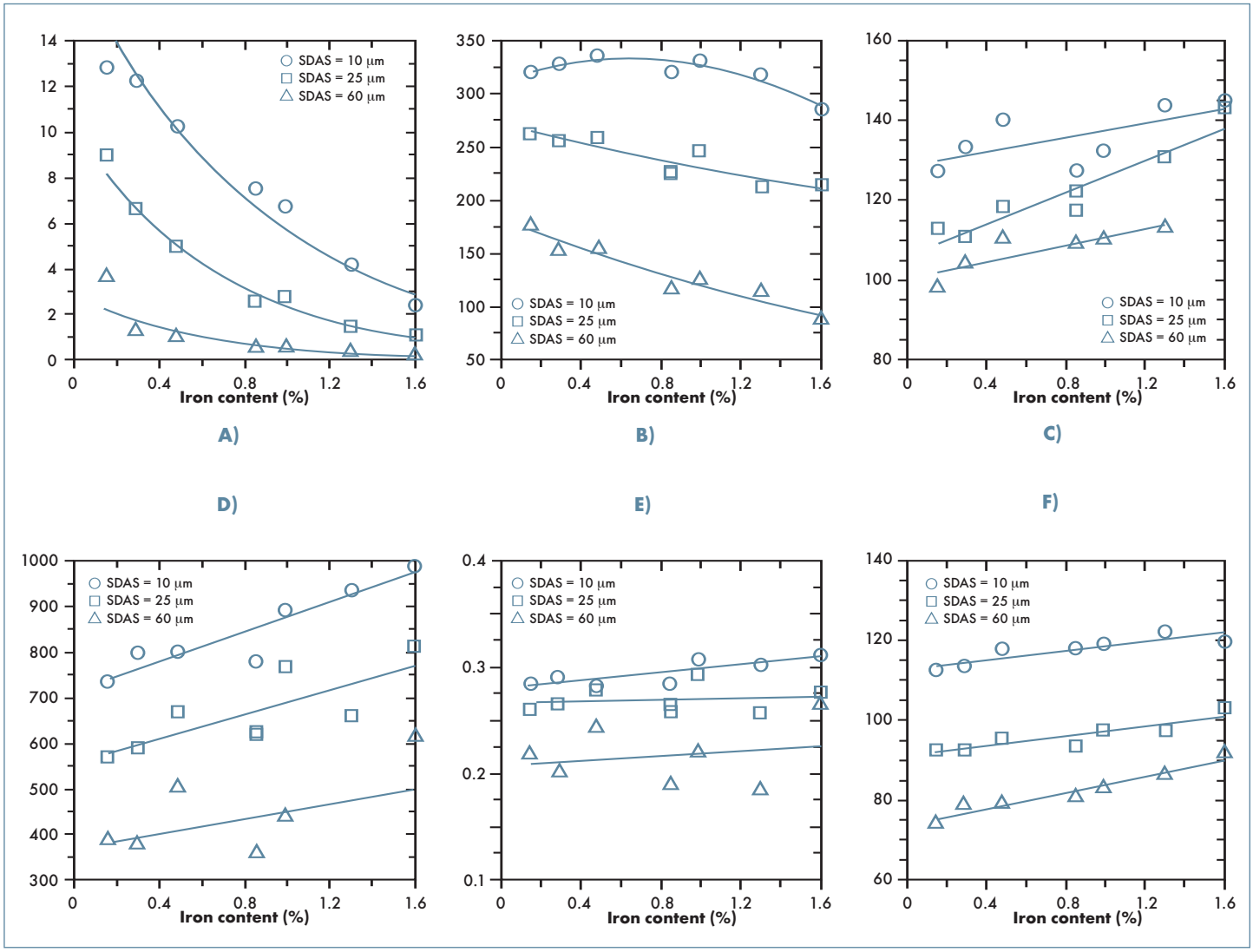

Fig. 5: Graphs showing the influence of iron level and cooling rate on the mechanical properties: a) elongation to fracture, b) ultimate tensile strength, c) yield strength, d) strength coefficient, e) strain hardening exponent and f) is macro Vicker´s hardness.

arrestment must have been taking place, slowing the damage sequences.

As the matrix work hardens, the overall stresses in the system rise. At a critical point, a crack can be initiated in one of the iron-rich plates, which are oriented perpendicular to the loading axis. Due to its inherent brittleness and the orientation of the plate, the crack will grow in an unstable manner along the length of the plate. In this case, a very large internal stress concentration will be produced due to this crack. The presence of this crack could either lead to immediate fracture by exceeding the critical stress intensity factor for the material or adjacent iron-rich intermetallics could be fractured, initiating micro cracks at these particles providing easy pathways for macro cracks to propagate through them leading to fracture of the bulk material. The needle-shaped Fe-bearing phase is therefore recognized as the most detrimental to the casting's mechanical properties why efforts should be dedicated to developing means of controlling the precipitation, growth and morphology of these harmful platelet-like β-Al_5FeSi intermetallic phases.

As demonstrated in figure 7, the mechanical properties are suffering a great loss as the length of these precipitates is increasing. They appear to be much more easily fractured under tensile loading than the aluminium matrix and/or the modified silicon particles, see appendix A, figure A2. Otherwise, if the silicon is unmodified, the cracks of silicon flakes are as prone to fracture and crack linkage as for the iron particles.

It is essential to mention that the β-Al_5FeSi platelets tend to be much more prone to fracture and crack linkage than the α-$Al_{15}(Fe,Mn)_3Si_2$-Chinese script particles. The current research elucidates that the influence of Mn on the tensile strength is beneficial. Concerning ductility, see table 4, there exist scatters in data making any correlations relatively poor in this case.

The reason for that is, as might be noted in table 2, the occurrence of predominant

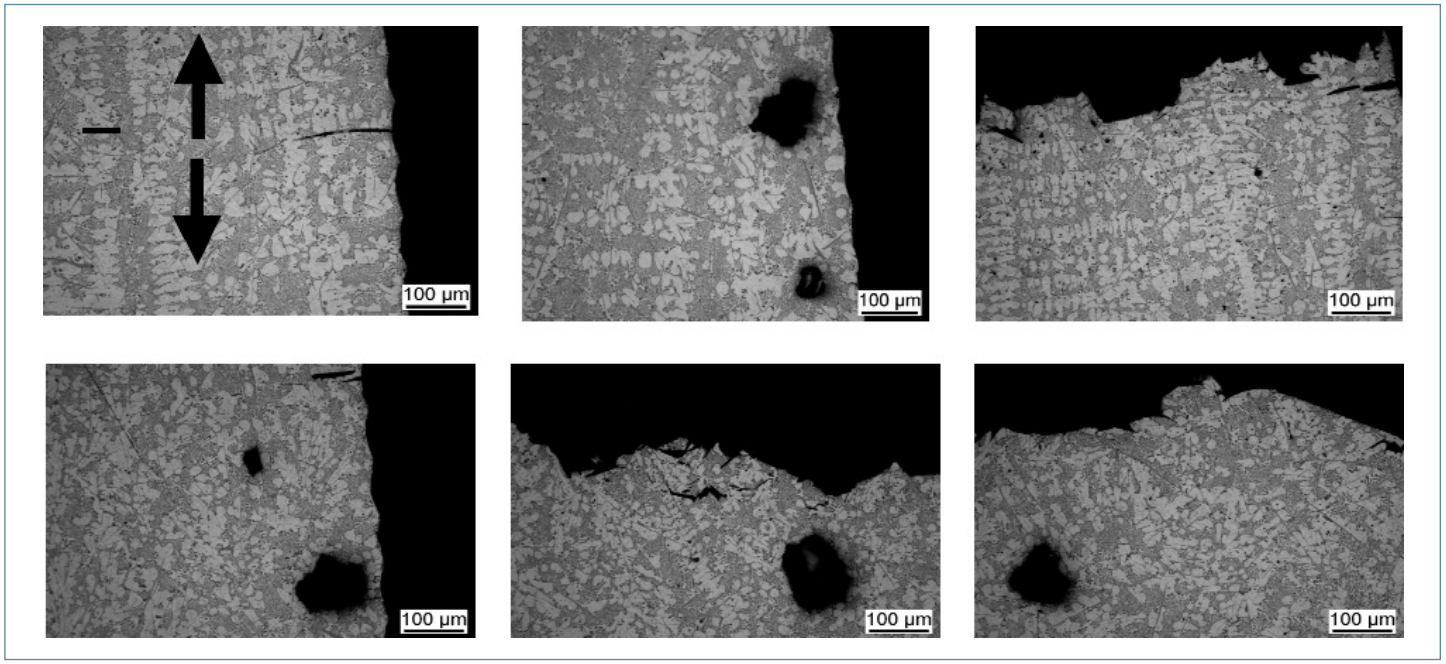

Fig. 6: Microstructural features illustrating the crack initiation and propagation of alloy 6 a-c and alloy 7 d-f for tensile samples of SDAS ~25 µm.

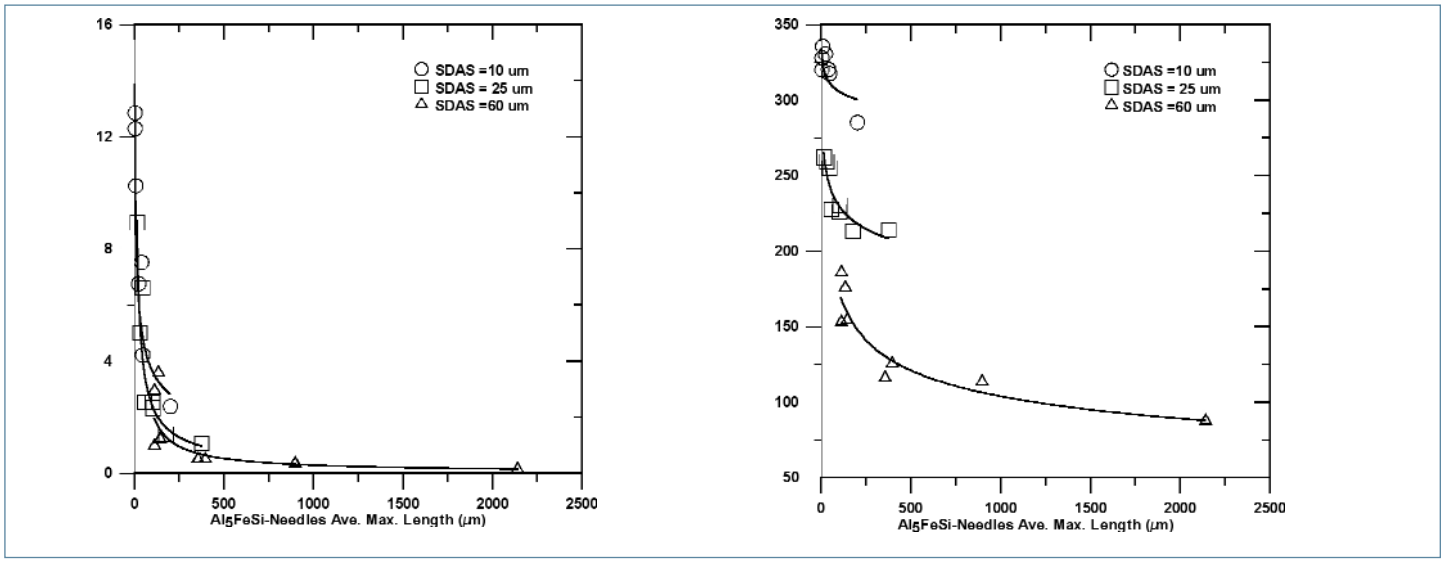

Fig. 7: Graphs illustrating the influence of the length Al5FeSi of on the tensile properties: a) elongation to fracture and b) the ultimate tensile strength.

Table 4. The influence of Fe, Mn and SDAS on the tensile properties.

		Ultimate tensile strength (MPa)			Elongation to fracture (%)		
Fe conc. w(%)	Mn conc. w(%)	SDAS: 7-10 µm	SDAS: 20-25 µm	SDAS: 50-60 µm	SDAS: 7-10 µm	SDAS: 20-25 µm	SDAS: 50-60 µm
0.29		328	255	155	12.3	6.6	1.2
0.85		320	226	116	7.5	2.5	0.5
1.30		317	213	113	4.2	1.4	0.4
0.35	0.15	339	265	153	10.2	6.4	1.2
0.79	0.34	315	271	149	5.7	4.4	0.7
1.10	0.50	323	209	158	4.4	1.6	0.9

iron-rich needles in the material still controlling the crack propagation and fracture process. It is also observed that when a Chinese script is fractured, the crack propagation appears to be arrested by the surrounding matrix, but as mentioned earlier, the needles are present and cracked, acting as linkage paths and facilitating the progression of damage.

CONCLUDING REMARKS

The relation between the level of iron, manganese and cooling rate on the microstructure formations and mechanical properties of a high pressure die cast alloy Al-9%Si-3%Cu has been investigated. The following conclusions are reached:

- At higher cooling rates and iron levels up to 0.2% the precipitation of large iron-rich particles seems to be suppressed or inhibited. At slow cooling conditions and higher iron levels, iron-rich phases might grow and coarsen, becoming some millimetres in size. The neutralization treatment of iron through addition of Mn did reduce the amount and volume fraction of the iron-rich needles but not suppress its formation or nullify it.
- At SDAS ~10 μm and levels up to 1%Fe and 0.5%Mn, few Chinese script $Al_{15}(Fe,Mn)_3Si_2$-phase where detected, instead some polyhedral and star like iron-rich compounds where observed. Generally, it has been found that the morphology, size and volume fraction of all types of intermetallics are dependent on the cooling rate, no matter if they precipitate as primary, binary or ternary reactions.
- The higher the iron concentrations the larger the loss of ductility; it seems to be associated with multi-cracking of the iron-rich particles by tensile loading independent of the cooling rate. At relatively higher iron levels, up to 1.3%, and 10 μm in SDAS, a slight enhancement of the ultimate tensile strength is likely to occur. At lower cooling rates, SDAS > 25 μm, remarkable reductions of the ultimate tensile strength are recorded gradually as the iron level is increased. Yield strength, strength coefficient and the strain hardening exponent exhibited an appreciable response to higher iron levels and cooling rates. Higher hardness values are approached as the iron level and cooling rate is increased. A slight enhancement in strength is observed as Mn is added in contrast to the elongation to fracture.
- No correlation could point out a degradation of the monotonic properties of Al-Si alloys caused neither by the length of the pore nor the area fraction of porosity. Instead, fracture and debonding of the iron-rich compounds, especially the iron-rich Al_5FeSi-needles appear to be responsible for the growth and coalescence of the cracks leading to premature fractures. The compact morphology of the Chinese scripts seems to inhibit the crack propagation since it is mostly surrounded by the ductile Al-matrix.
- Increasing the iron concentration, the inability of the liquid metal to feed the interdendritic regions becomes more apparent resulting in the formation of shrinkage cavities. But note, no correlation has been detected between the amount of iron in the melt and the size and area fraction of porosity. Instead, clear evidences show that there exist a relation between the cooling rate and the formation of porosity.

ACKNOWLEDGEMENT

The authors acknowledge the Swedish Governmental Agency for Innovation Systems (VINNOVA) for financially sponsoring the project.

APPENDIX A

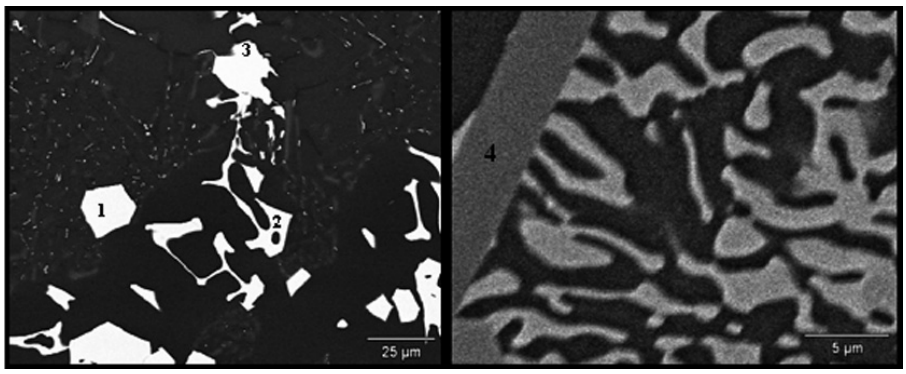

Fig. A1 Alloy 11: Different iron-rich phases marked as 1 for the polyhedral morphology, 2 for the Chinese script morphology, 3 for the more compact star-like iron-rich compound and 4 is the iron-rich needle phase.

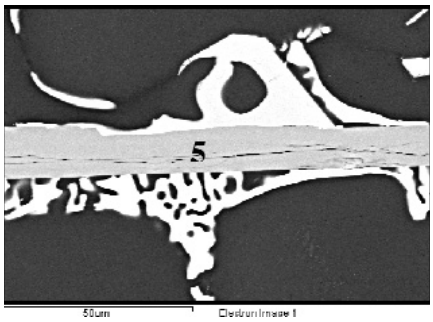

Fig. A2: SEM picture showing the cracks in the centre line of the Al5FeSi-needle, alloy 4.

Table A1. The chemical composition of the different iron-rich phases that are numbered in figures A1 and A2.

Phase No.	Element (weight %)					
	Al	Si	Mn	Fe	Cu	Total
1	58.75	9.24	14.44	16.20	1.37	100.00
2	62.49	8.90	12.66	14.55	1.40	100.00
3	57.85	8.91	12.35	17.30	3.59	100.00
4	56.07	17.65	6.08	20.20		100.00
5	59.26	16.29		24.45		100.00

REFERENCES

[1] L. Wang, D. Apelian, One Hundred Third Annual Meeting of the American Foundrymen's Society, (1999) pp. 231-238.

[2] S.G. Shabestari, J.E. Gruzleski,, Cast Metals, vol. 6, no. 4 (1994) pp. 217-224.

[3] Z. Ma, A.M. Samuel, F.H. Samuel, AFS Transactions, (2004) pp. 131-140.

[4] S. Gowri, F.H. Samuel, Metallurgical and Materials Transactions A, vol. 25A, no. 2 (1994) pp. 437-448.

[5] P.N. Crepeau,, AFS Transactions (1995) pp. 361-366.

[6] A.M. Samuel, A. Pennorst, C. Villeneuve, F.H. Samuel, H.W. Doty and S. Valtierra,, International Journal of Cast Metals Research, vol. 13, (2000) pp. 231-253.

[7] L. Lu, A.K. Dahle, Metallurgical and Materials Transactions A, vol. 36A, (2005) pp. 819-835.

[8] N. A. Belov, A.A. Aksenov, D.G. Eskin, Advances in Metallic Alloys, A series edited by J. N. Fridlander and D.G. Eskin, 2002.

[9] Pennors, A.M. Samuel, F.H. Samuel, H.W. Doty, AFS Transactions, (1998) pp. 251-264.

[10] G. Gustafsson, T. Thorvaldsson, G.L. Dunlo, Metallurgical Transactions A, vol. 17 A, (1986) pp. 45-52.

[11] A.M. Samuel, F.H. Samuel, C. Villeneuve, F.H. Samuel, H.W. Doty and S. Valtierra, International Journal of Cast Metals Research, vol. 14, (2001) pp. 97-120.

[12] J.A. Taylor, G. B. Schaffer, D.H. StJohn, Metallurgical and Materials Transactions A, vol. 30 A, (1999) pp. 1651-1655.

[13] S. Sreeja Kumari, R. M. Pillai and B. C. Pai,. Indian foundry journal, (2002).

[14] X. P. Niu, B.H. Hu, S.W. Hao, J. of materials science letters, vol. 17, no. 20 (1998) pp. 1727-1729.

[15] S.G. Shabestari, M. Mahmudi, M. Emamy, J. Campbell, International Journal of Cast Metals Research, vol. 15, no. 1 (2002) pp. 17-24.

[16] S.G. Shabestari, Materials Science and Engineering A, vol. 383 (2004) pp. 289-298.

[17] C.M. Dinnis, J.A. Taylor, A.K. Dahle, D.H. StJohn, W. Schneider, Light Metals (Metaux Legers) 2003: International Symposium on Light Metals as held at the 42nd Annual Conference of Metallurgists of CIM (COM 2003); Vancouver; Canada, (2003) pp. 483-497.

[18] J.A Taylor, G.B. Schaffer, D.H. StJohn, Metallurgical and Materials Transactions A, vol. 30A (1999) pp. 1643-1650.

[19] J.A Taylor, G.B. Schaffer, D.H. StJohn, Metallurgical and Materials Transactions A, vol. 30A (1999) pp. 1657-1662.

[20] P.S. Mohanty, F.H. Samuel, J.E. Gruzleski, AFS Transactions, (1995) pp. 555-564.

[21] G. Boudreault, A.M. Samuel, F.H. Samuel, H.W. Doty, AFS Transactions, (1995) pp. 207-216.

[22] N. Roy, A.M. Samuel, F.H. Samuel, Metallurgical and Materials Transactions A, vol. 27A (1996) pp. 415-429.

[23] Z. Li, A.M. Samuel, F.H. Samuel, C. Ravindran, S. Valtierra, H.W Doty, Materials Science and Engineering A, vol. 367, issues 1-2 (2004) pp. 96-110.

[24] H. Cáceres, M.B. Djurdjevic, T. J. Stockwell, J.H. Sokolowski, Scripta Materialia, vol. 40, no. 5 (1999) pp. 631-637.

[25] G. A. Edwards, G.K. Sigworth, C.H. Cáceres, D.H. StJohn, J. Barresi, AFS Transactions, (1997) pp. 809-817.

[26] Tian, J. Law, J. Van der Touw, M. Murray, J.Y. Yao, D. Graham, D. StJohn, Journal of materials processing technology 122, (2002) pp. 82-93.

[27] S. K. Tang, T. Sritharan, Materials Science and Technology, vol. 14 (1998) pp. 738-742.

[28] P. Kumar, J.L. Gaindhar, AFS Transaction, (1997) pp. 635-638.

[29] L. Bäckerud, G. Chai, Jarmo Tamminen, Solidification characteristics of aluminium alloys, vol.2, Stockholm, (1990), ISBN 0 87433 119 6.

[30] B.Suares-Pena and J. Asensio-Lozano, Scripta Materialia, vol. 54, issue 9 (2006) pp. 1543-1548.

[31] M.Mahta, M. Emamy, A. Daman, A. Keyvani and J. Campbell, International Journal of Cast Metals Research, vol. 18, no. 2, (2005) pp. 73-79.

[32] S. K. Tang, T. Sritharan, Materials Science and Technology, vol. 14 (1998) pp. 738-742.

[33] T.S. Shih, L. W. Hang and Y. J. Chen, International Journal of Cast Metals Research, vol. 18, no. 5 (2005) pp. 301-308.

[34] Campbell J, Castings, 2nd Ed, Butterworth-Heinemann Ltd, Oxford (2003), ISBN 0 7506 4790 6.

[35] Q.G. Wang, Metallurgical and Materials Transactions A, vol. 34A (2003) pp. 2887-2899.

[36] G. Guiglionda and W.J. Poole, Materials Science and Engineering A, vol. 336, issues 1-2 (2002) pp. 159-169.

[37] M. Avalle, G. Belingardi, M.P. Cavatorta and R. Doglione, International journal of Fatigue, vol. 24 (2002) pp. 1-9.

[38] C.H. Cáceres and B.I. Selling, Materials Science and Engineering A, vol. 220, issues 1-2 (1996) pp. 109-116.

[39] M. Harada, T. Suzuki and I. Fukui, Journal of the Japan foundrymen´s society, vol. 55, no. 12 (1983) pp. 47-50.

[40] M.K. Surappa, E. Blank and J.C. Jaquet, Scripta Metallurgica, vol. 20, no. 9 (1986) pp. 1281-1286.

[41] J.G. Conley, J. Huang, J. Asada and K. Akiba, One Hundred Third Annual Meeting of the American Foundrymen's Society, (1999) pp. 737-742.

[42] C.H . Cáceres , Scripta Materialia, vol. 32, no.11 (1995) pp. 1851-1856.